Measuring Ice Hockey Shot Accuracy with Precision: A 3D Puck Flight Simulation

Aaron Manning

Department of Kinesiology and Physical Education

McGill University

Montréal, Québec, Canada

A thesis submitted to McGill University in partial fulfilment of the requirements of the degree of Master of Science

Abstract

Shot accuracy is a crucial metric in the game of ice hockey, yet rarely quantified with high precision. Due to limitations imposed by the large capture volume, it is not practical to use 3D motion capture techniques to simultaneously record body kinematics and puck trajectory to measure shot accuracy. Hence, this study's purpose was to develop a computational model to predict ice hockey shot trajectory based on the initial puck launch vectors and aerodynamic variables. Using 3D puck trajectory motion data collected from dynamic wrist and slap shots executed on ice, the puck's position and orientation were measured from release to an end target location. The measured position at the target was used to assess the model's ability to predict puck trajectory. The puck flight model for shots travelling over 6 m and 10 m was accurate in predicting puck-to-target positions within 5 cm mean absolute error (less than a puck's diameter). Refinement of aerodynamic coefficients and inclusion of the Magnus side force could further improve the precision of the model. Ultimately, players and coaches could use this predictive model in combination with a puck launch vector measurement system as a training tool to evaluate player shot accuracy both on ice and in smaller off-ice training facilities.

Abrégé

Dans le sport de hockey sur glace, la précision du lancer est une mesure importante, mais celui-ci est rarement quantifié avec haute exactitude. En raison de limitations imposés par les volumes de capture des caméras 3D, il n'est pas pratique de collectionner les kinématiques du corps et la trajectoire de la rondelle simultanément. Par conséquent, l'objectif de cette étude était de développer un modèle informatique pour prédire la trajectoire de lancer de hockey sur glace basé sur les vecteurs de lancement initial et les variables aérodynamique. En utilisant les trajectoires kinématiques 3D de rondelle de lancé-frappé et lancé du poignet dynamique sur glace, la position et orientation de la rondelle a été mesuré de la libération de la lame à la location finale d'une cible. C'est data ont étés utiliser pour évaluer la capacité du modèle à prédire la trajectoire de la rondelle. Le modèle de vol de la rondelle pour les lancés de distance de 6m et 10m a prédit les positions de rondelle-cible avec une exactitude de moins de 5cm d'erreur absolu (moins du diamètre d'une rondelle). Le raffinement des coefficients aérodynamique et l'inclusion de la force de côté Magnus pourrait améliorer l'exactitude du modèle. Finalement, les joueurs et entraineurs pourrait utiliser ce modèle prédictif en combinaison avec les mesures de rondelles avec capteur intelligent comme outil d'entrainement pour l'évaluation de précision de lancés des joueurs sur la glace et aussi dans les plus petites installations hors-glace.

Acknowledgements

I would firstly like to thank Dr. David Pearsall for giving me the opportunity to begin a new path in sports biomechanics research, through this Master's degree in the Ice Hockey Research Group. You have encouraged me to pursue my passion for sport and science, both inside and outside the world of hockey, and provided guidance and support at every turn. Phil Renaud, I couldn't have done this project without your continuous dedication throughout data collection, as well as the analysis and writing process.

To all of the lab mates I've studied with – you have been the reason I had so much fun doing this degree. Dan, Neil, Mike – you made me feel like part of the family from day one and I can't thank you enough for that. Caitlin, Sean, Aimée (whose coffee brewing took a month off the time it took to finish this thesis), and Lily – your friendship has got me through the grind of graduate student life and made my time in Montreal a memory I will always cherish. And to Matt and my (human) roommates Taylor and Harry – thanks for continuing the tradition of camaraderie, inside and outside the lab. The IHRG is in good hands.

Lastly, I would like to thank my parents for their absolutely unwavering support through my seemingly crazy decision to leave my job and pursue graduate school. In the most sincere sense of the phrase, I could not have done this without you.

Contribution of Authors

Aaron Manning, MSc candidate, Department of Kinesiology and Physical Education, McGill University, was responsible for the research design, data processing and analysis, writing of all codes required to run the simulation, and the writing of this thesis. The candidate's supervisor, David J. Pearsall, PhD, Associate Professor, Department of Kinesiology and Physical Education, McGill University, advised on the research design, data collection methods and analysis of data.

Dr. Mark Driscoll, Professor, Department of Mechanical Engineering, McGill University, and Dr. Larry Lessard, PhD, Professor, Department of Mechanical Engineering, McGill University, sat on the thesis advisory committee and provided feedback on the research design proposal.

Philippe J. Renaud, MSc, Department of Kinesiology and Physical Education, McGill University, played a crucial role in data collection, including recruitment of participants and setup and calibration of the motion capture system, acting as the lab's research assistant. Neil MacInnis, MSc, Department of Kinesiology and Physical Education, McGill University, also played a critical role in all data collection procedures as a Master's student. Data collection was also aided by Sean Denroche, Aimée Quintana, Caitlin Mazurek and Michael Solomon, all students in the Department of Kinesiology and Physical Education, McGill University.

Contents

List of Figures

List of Tables

Variable Definitions and Notation

Vectors, matrices and tensors are in **bold**

Constants and variables are in *italics*

Direction vectors are denoted with ^

All units are SI unless otherwise stated

A_p – surface area of the puck (m^2)

C_D – drag coefficient (unitless)

C_L – lift coefficient (unitless)

C_M – pitch torque coefficient (unitless)

C_N – spin decay coefficient (unitless)

CI – confidence intervals

D_x, D_y, D_z – the model's error in prediction of final position of the puck's center of mass (m)

E_x, E_y, E_z – final position of the puck's center of mass, estimated by the simulation (m)

F – force (N)

g – acceleration due to gravity (m/s^2)

I_P – inertia tensor of the puck (kg m^2)

m_p – mass of the puck (kg)

M_x, M_y, M_z – final position of the puck's center of mass, as measured by optical motion capture (m)

r – position of the puck's center of mass (m)

r_p – radius of the puck (m)

RH – local relative humidity of air (%)

SD – standard deviation

T – local air temperature (ºC)

v – linear velocity (m/s)

V-N-S – positions in the wind co-ordinate system (m)

W - quaternion rate matrix (unitless)

X-Y-Z – positions in the global co-ordinate system (m)

X’-Y’-Z’ – positions in the puck’s body-fixed local co-ordinate system (m)

α – angle of attack (degrees)

β – spatial orientation of the puck, expressed as an Euler quaternion (unitless)

ρ – air density (kg/m^3)

τ – torque (kg m)

ω – angular velocity (rad/s)

1 – Introduction

The wrist shot and slap shot are two crucial skills in the game of ice hockey. Players seek to maximize the potential for goal scoring by increasing the speed and accuracy of their shots. Many studies have sought to identify the equipment, movement patterns and kinetics that produce shots with the highest speed [1–4]. However, few studies have investigated the biomechanical factors that contribute to shot accuracy, and those studies have used simple binary (hit or miss) outcome measures to quantify shot accuracy [5, 6].

Accuracy has been studied and precisely quantified in sports like pistol shooting, using metrics such as mean absolute radial distance from a target, RMS distance from a target and shot spread size [7–9]. The likely reason that accuracy has not been quantified in ice hockey with high spatial resolution is the challenging nature of measuring final shot position relative to a target.

Measuring puck position with video analysis would be inaccurate and time-consuming. More accurate results can be obtained by fixing a reflective marker to the puck and tracking its motion using optical motion capture [5, 6]; however, this requires a substantial number of cameras to track movement within the large spatial envelope (e.g.17 m long x 7 m wide x 2 m high) traversed by the player and puck flight. A given number of cameras has a finite capture volume, so researchers measuring player's body kinematics have only been able to track the puck motion for the initial portion of its trajectory [5, 6, 10].

Hence, the purpose of the current study was to develop and validate a computer simulation to model puck trajectory based on initial launch conditions. Ultimately, this model can be used to determine the final position of a puck relative to a target, based on measurements from the first 1 to 2 meters of the puck's flight.

2 – Literature Review

2.1 – Ice Hockey Shooting

In ice hockey, shooting has been identified by professional scouts as the game's second most important skill [11]. Shooting outcomes are assessed via two measures: how fast the puck is traveling (i.e. shot speed), and how closely the puck approaches the preferred target (i.e. shot accuracy). Shot speed has been used as the single shooting outcome measure in investigations of stick shaft stiffness [1, 4] and shaft deflection during the shot [3]. Additionally, shot speed has been shown to correlate with player skill level [3, 10]. Shot speed has been measured by means of a radar gun [3, 4], accelerometer placed inside a puck [2] and through the tracking of a single passive reflective marker instrumented on the puck [1, 10]; however, few studies have quantified shot accuracy.

Michaud-Paquette, Magee, Pearsall, & Turcotte conducted a series of 3D kinematic ice hockey shot studies, focusing on whole-body predictors of shooting accuracy [5, 6]. An eight-camera motion capture system was used to record participants' body and stick kinematics. On a synthetic ice surface within a lab, participants performed shots aimed at 0.3×0.3 m targets located at each corner of a hockey net, from a distance of four meters. Accuracy score was recorded as a percentage of successful shots that passed through the target – each shot was recorded as either a "hit" or "miss". This binary method is adequate for identifying gross body mechanics that influence shot accuracy [6] but lacks resolution in terms of spatial puck to target measures.

In Michaud-Paquette, Magee, Pearsall, & Turcotte's shooting studies, reflective markers were fixed to the puck and the motion of the puck was tracked by the motion capture system throughout the flight [5][6]. Shots travelled 4 meters from release to target, allowing the eight-camera system to contain the entire flight within the capture volume. However, goal-scoring shots in ice hockey game play occur from anywhere in the offensive zone (the area of the ice from the blue line to the net) [12]. Therefore, shots can travel up to 19 meters from release to target.

To the best knowledge of this author, no study has investigated shooting accuracy in ice hockey for shots taken on ice or over distances greater than four meters. This could be due to the difficulty and impracticality of tracking a puck using 3D motion capture for long shots; tracking a shot's entire trajectory over long distances would require a substantial number of cameras. However, using motion capture data collected within a delimited volume, a simulation model of puck flight could be used to estimate shot trajectory over a range of shot distances.

2.2 – Accuracy Metrics

In accuracy-based sports such as archery and pistol shooting, shot accuracy has been quantitatively studied and measured. Athletes performing these sports attempt to minimize the deviation of their shots from a preferred target and seek techniques which maximize repeatability. Accuracy for a group of shots has been quantified by mean absolute radial distance from a target [8], RMS distance from the target [8], grouping size (radial distance between the two farthest shots in a group) [13] and standard deviation in the vertical and lateral directions [7]. These outcome measures have been used to study the effects of vision correction [7, 8], postural stability [8] and multi-joint coordination patterns [9] on shot accuracy in pistol shooting. These studies are beneficial to athletes seeking to maximize accuracy as they identify the attributes and movement patterns of successful shooters.

Accuracy has also been extensively studied from the perspective of motor control. Fitts' Law states that the time it takes to perform a task with an accuracy-based goal is a function of the distance to the target and the size of the target [14]. A target that is smaller and farther away will increase the time it takes a person to aim at the target. Fitts initially showed this phenomenon using a pointing task with a stylus [14], but the model has been shown to be valid in other tasks involving speed and accuracy including video games [15] and pistol shooting [16].

If these metrics were adopted in ice hockey, they could offer athletes and coaches crucial feedback on player performance. The metrics would offer a more precise quantification than the binary (hit/miss) method used by Michaud-Paquette et al. [5, 6] and inform the coaches and players about the magnitude and direction of their misses. Additionally, these metrics could be used by future researchers to determine the kinematics, joint co-ordination or equipment variables that contribute to shot accuracy.

2.3 – Sport Projectile Flight Modelling

With increased funding for sport sciences in recent years, studies of sport projectiles have become more ubiquitous. A review article on the aerodynamics of projectiles in sport indicates that studies on at least 18 different sports projectiles have been published in the past 20 years [17]. Aerodynamic parameters of sports projectiles can be estimated using computational fluid dynamics (CFD) [18] or directly measured using wind tunnel testing. Wind tunnel testing is considered the “gold standard” for determination of aerodynamic parameters, while CFD is a lower-budget option [17].

In addition to the gravitational force on a projectile in flight, one must also consider the aerodynamic forces acting on the projectile. For non-rotating objects such as airplane wings, the aerodynamic forces are drag (the aerodynamic force that acts anti-parallel to the object’s velocity) and lift (the force that acts perpendicular to velocity). If the object is rotating, an additional force called the Magnus force must be considered (Fig. 1). This force acts in the direction perpendicular to both the rotation axis and the projectile’s velocity [17]. This is the force that causes a golf ball with side-spin to “slice” or “hook”, and is also the force that causes batted baseballs with back-spin to rise, resulting in longer flight trajectories. The Magnus force is caused by a pressure differential between the leading edge and trailing edge of the projectile. This arises because the leading edge “pulls” air along due to fluid friction and causes a local increase in the air’s velocity, and therefore a local decrease in pressure. Magnus force coefficients have been measured using wind tunnel testing on soccer balls [19], baseballs [20], rugby balls [21] and other sports projectiles [17]. Magnus forces have also been quantified using high speed video analysis on baseballs [22] and soccer balls [23]. Fig. 1 shows the direction of the aerodynamic force vectors for a ball in flight with back-spin.

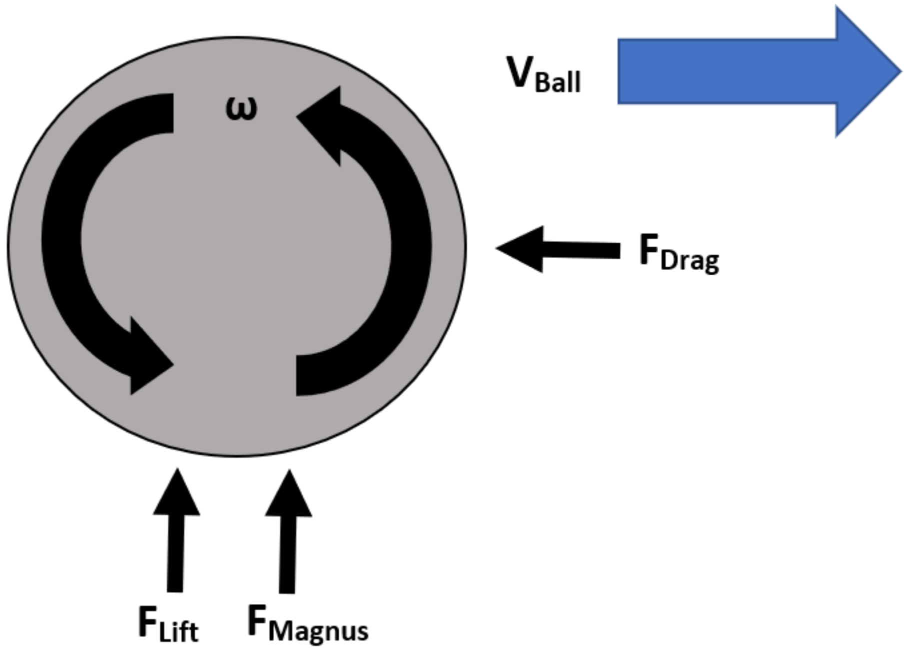

Fig. 1 Aerodynamic forces on a spinning projectile in flight. The figure shows a ball with back-spin and the direction of the aerodynamic force vectors. Drag acts in the opposite direction of the ball's velocity, lift acts perpendicular to drag and the Magnus force acts in the ω x v direction, which is the same direction as lift in the case of a ball with pure back-spin.

In addition to the aerodynamic forces on a projectile, the aerodynamic moments that cause changes to the orientation of the object must be considered. The pitching moment is the moment that acts along the pitch axis of a body, arising from the fact that the location of aerodynamic force application (the center of pressure) is not the same as the object's center of rotation [17]. This moment arm gives rise to a torque about the pitch axis of the object. In the case of an ice hockey puck in flight, the pitching moment acts in a direction to increase the angle of attack (the angle between the puck's orientation and the relative wind velocity).

For rotating projectiles, the spin down moment is the moment that causes the rotational velocity of the object to decrease throughout flight. This is caused by local air friction around the rotating edges of the projectile. It has been observed that the spin down moment causes a batted baseball to land with 25% of its original rotational velocity [17]. Spin down moment is measured empirically by observing the rate of spin decay, often using high-speed video analysis [17] [24].

2.4 – Ice Hockey Puck Flight Simulation

Böhm, Schwiewagner, & Senner were the first to simulate ice hockey puck flight in 2007 [24]. The purpose of their study was to simulate shot trajectories to determine optimal glass and board barrier height for spectator safety. Drag, lift, and pitch moment coefficients were determined using wind tunnel testing of a hockey puck as a function of angle of attack, between 0º and 80º. Initial take off conditions including angle of attack, velocity and spin rate were then measured for 108 shots taken by professional ice hockey players in a lab environment. Shots were recorded using a six-camera Vicon motion capture system. Observed initial take off conditions and corresponding drag and lift coefficients were used to solve the Newton–Euler differential equations for a rigid body to simulate puck flights from multiple positions on the ice surface. 8415 shots were simulated for each barrier height. The authors used the simulation to determine the percentage of pucks that would go over the barrier at any given barrier height.

To validate their simulation, all experimentally measured shots were compared to simulated puck trajectories. For shots with a trajectory length of 3 meters, final puck locations estimated by the simulation differed from the measured puck flight data by an average of 0.06 ± 1.38 cm in the vertical direction and -0.33 ± 0.72 cm in the lateral direction. However, the model was only verified for a maximum shot distance of 3 meters, whereas a large proportion of shots taken in hockey games are taken from greater distances [12].

2.5 – Analysis of Predictive Models

Two of the most popular metrics to describe the accuracy of a predictive model are mean absolute error (MAE) and root mean squared error (RMSE). Both metrics are commonly used in predictive models for meteorology, air quality and climate research studies [25]. MAE is the average absolute difference between a model's prediction and the actual outcome, while RMSE is the square-rooted sum of squared differences between prediction and outcome. MAE gives equal weight to all measurements, while RMSE gives higher weight to errors with greater magnitude, effectively "penalizing" models with higher variance or models that are prone to producing outliers [25]. There is debate over which metric is more appropriate for evaluating predictive models. It is argued by Wilmott et al. that MAE is less ambiguous and more natural and easily interpreted than RMSE [26]. Conversely, it is argued by Chai et al. that RMSE is more appropriate because penalizing large errors is effective in improvement of model performance [25].

Bland-Altman analysis is a statistical technique for comparison of two different quantitative measurement methods, commonly used in the medical sciences to compare novel measurement techniques to established methods [27]. Bland-Altman analysis compares the mean differences between the measurement techniques and establishes the limits of agreement, the interval where a defined percentage (typically 95%) of the differences between measurements are expected to lie [27]. Bland-Altman analysis is also effective in determining whether a measurement method has bias (ie. whether it tends to overestimate or underestimate the true value of interest). Additionally, Bland-Altman analysis can be combined with regression analysis to investigate a method's proportional bias [27].

Bland-Altman analysis simply defines the limits of agreement between measurement techniques but does not define whether the investigated measurement technique is acceptable. The acceptable limits must be defined by the researcher or clinician based on the goals of the measurement technique [28].

3 – Objectives and Hypotheses

Recent studies have shown the feasibility of collecting 3D motion data of ice hockey skating [29] and shooting [30] tasks on an ice surface and over large fields of view [31]. Hence, it is possible to measure puck trajectories to validate a puck flight simulation model in realistic conditions: on ice, for shots travelling distances observed in ice hockey game play.

A validated puck flight simulation model could offer a practical solution to quantifying shooting accuracy with high spatial resolution. Puck flight can be modeled to intersect a target's plane, thus rendering the location of the puck relative to the middle of a target. As model calculations would be based on initial launch conditions, an extended camera field of view would not be needed to measure puck trajectory from launch to net. This model could be used for athletes and coaches to provide quantitative shooting accuracy metrics and ultimately improve shooting performance. Hence, the objective of the current study was to develop a model to predict ice hockey shot trajectory based on the initial puck launch vectors and aerodynamic variables and to assess its precision and accuracy on-ice across distances of 6 and 10 meters.

Based on the results of Bohm et al.'s simulation [24], it is expected that the model will predict the final puck position in the vertical and lateral directions with a mean absolute error of less than 0.5% of the total flight path. This corresponds with an expected mean absolute error of 3 cm for shots travelling 6 meters and 5 cm for shots travelling 10 meters.

It is further hypothesized that the model will predict wrist shots and slap shots with equal accuracy. Additionally, it is hypothesized that the model's accuracy will not be significantly different for right-handed shooters (RHS) and left-handed shooters (LHS).

4 - Methods

4.1 – Data Collection Protocol

Nine experienced ice hockey players (age 26.6 ± 3.2 years, height 180.7± 7.4 cm, mass 88.3 ± 10.8 kg, playing experience 21.3 ± 3.5 years) participated in the study. Six participants were LHS and three participants were RHS. Participants' highest playing experience level varied from high school to university varsity. Prior to testing, all participants read and signed a consent form in accordance with McGill University Research Ethics Board II.

Testing occurred on ice at McGill University's McConnell Arena. Participants wore their own skates and gloves, and were provided sticks (2S and 1X 95 flex with P92 blade pattern) from Bauer Hockey LLC (Blainville, QC, Canada). Prior to the shooting protocol, participants were allowed a ten minute warm-up period, in which participants were instructed to practice skating and taking wrist shots and slap shots aimed at a net.

Participants were then instructed to perform a series of dynamic wrist and slap shots aimed at a target, as seen in Fig. 2. For each shot, the target was either placed in the "near" position or the "far" position. The target was a black circular foam pad with a diameter of 32.7 cm, mounted on a vertical post. The height from the ice surface to the center of the target was 76 cm. Near shots were made with the target 7.5 m from the end of the release zone, to simulate a shot from the "slot" (a high-scoring area on the ice in front of the net between the hashmarks and top of the faceoff circles [12]). Far shots were made with the target 15 m from the end of the release zone, to simulate a shot from the "point" (the area between the top of the circles and the blue line at which long distance shots are often executed [12]).

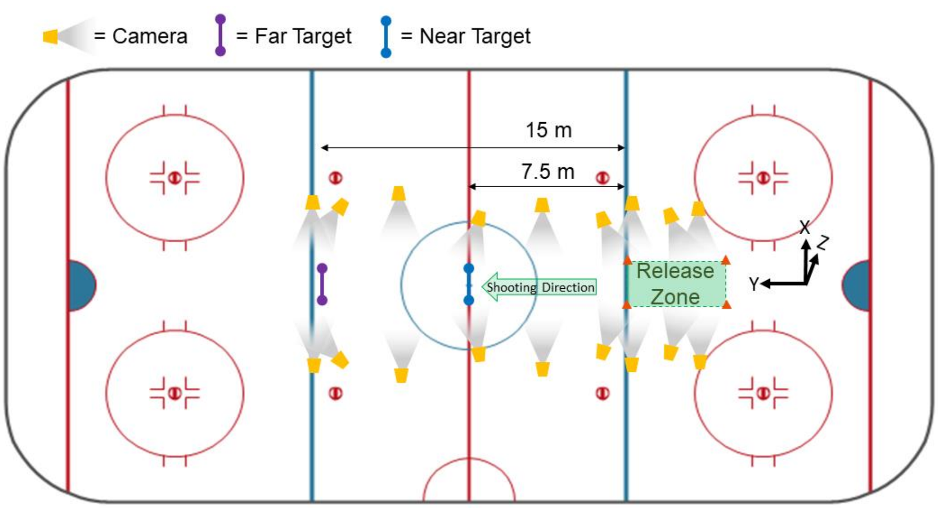

Fig. 2 Top view of the testing protocol set-up: A release zone was marked with orange pylons. Targets were positioned 7.5 (near target) and 15 (far target) meters from the end of the release zone. The global co-ordinate system is presented where +Z is perpendicular to the ice surface

Participants were instructed to perform shots with optimal speed and accuracy, as if they were attempting to score a goal in a game situation. For slap shots, participants started skating from rest and executed two to three strides inside the "release zone" before striking the stationary puck placed on the blue line at the edge of the release zone.

For wrist shots, participants began with the puck and were instructed to execute two to three strides before releasing the shot at the end of the release zone. Table 1 shows the number of shots by condition performed by each participant, for a total of 40 shots.

Table 1 Shooting test protocol performed by each participant

Repetitions	Shot Type	Target Distance
20	Wrist	Near
5	Wrist	Far
10	Slap	Near
5	Slap	Far

4.2 – Instrumentation

An 18-camera passive motion capture system (Vicon Motion Systems Ltd., Oxford, UK) operating at 240 Hz was set up on the ice surface and used to track motion of the puck. Cameras were mounted on tripods and connected to a Vicon Giganet connection hub and desktop computer. Prior to each participant's set of shots, the cameras were calibrated to capture a volume of approximately 17 m long x 7 m wide x 2 m tall.

Custom pins with 8 mm diameter, covered in retro-reflective tape (3M, St. Paul, MN, USA), were anchored to the puck and used as reflective markers. The markers were placed in a 50 x 40 x 30 mm scalene triangle configuration, with the midpoint of the triangle's base at the puck's center, as shown in Fig. 3. Marker positions were used to calculate the position and orientation of the puck for each frame throughout the puck's flight. Markers placed on the perimeter of the target were used to measure the position of the target.

Fig. 3 Instrumented puck with retro-reflective markers placed in a scalene triangle

4.3 – Data Processing

Marker position data were labelled and gap-filled using Vicon Nexus (Ver 2.5.0, Vicon Motion Systems Ltd., Oxford, UK) software. Data were exported and further analysis was performed in MATLAB R2019a (The MathWorks Inc., Natick, MA, USA). Position data were filtered with a 4^{th} order low-pass Butterworth filter with a cutoff frequency of 50 Hz.

For each frame, marker position data were used to calculate the position of the puck's center of mass $\boldsymbol{r}$ and the spatial orientation of the puck, expressed as an Euler quaternion $\boldsymbol{\beta}$ [32]. Puck velocity $\boldsymbol{v}$ and angular velocity $\boldsymbol{\omega}$ were calculated by taking the first derivatives of $\boldsymbol{r}$ and $\boldsymbol{\beta}$, respectively. Shot release was defined as the frame in which maximum magnitude of puck velocity occurred.

The puck flight model used the position, orientation, velocity and spin rate of the puck during the "initial flight phase" to simulate the complete trajectory of the puck's flight. Initial flight phase began 20 ms after the puck's maximum recorded velocity, and lasted 54 ms (13 frames of data at 240 Hz). This 20 ms lag between maximum puck velocity and initial flight phase ensured the puck was no longer in contact with the stick. Initial puck position was the location of the puck's center of mass in the first frame following release. Orientation and velocity were calculated for each frame in the initial flight phase and their average values were input to the model. Spin rate was calculated by taking a time derivative of the puck's orientation quaternion using the method defined by Diebel [32], and the average value during initial flight phase was input into the model.

4.4 – Puck Flight Model

4.4.1 – Co-ordinate Systems

Fig. 4 shows the co-ordinate systems used in the simulation. In the global co-ordinate system, +Z was defined as perpendicular to the ice surface and +Y was defined as the vector perpendicular to the plane of the target, intersecting the center of the target. In the puck's body-fixed co-ordinate system, +Z' was defined as the vector normal to the surface of the puck, aligned with global +Z when the puck is lying flat on the ice. +Y' was arbitrarily defined as the direction of initial velocity. In the wind co-ordinate system, the puck's velocity defines the +V direction, and +N is perpendicular to V in the plane defined by V and Z. +X, +X' and +S were determined using the right hand rule for their respective co-ordinate systems.

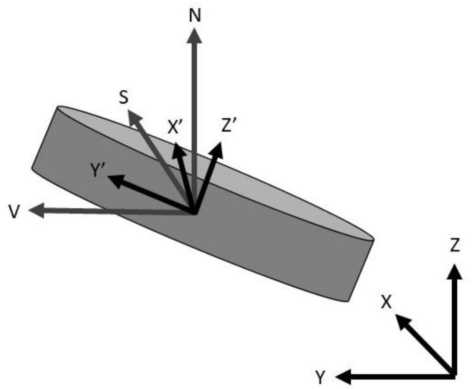

Fig. 4 Global (X-Y-Z), Body (X'-Y'-Z') and Wind (N-V-S) co-ordinate systems, adopted from Bohm et al. [24]

4.4.2 – Governing Equations

The puck's trajectory is described by the Newton-Euler equations for a rigid body in flight. MATLAB R2019a's "ode45" function was used to solve the set of coupled differential equations, defined in equation (1):

$$\frac{d}{dt}\begin{pmatrix} \boldsymbol{r} \\ \boldsymbol{\beta} \\ \boldsymbol{v} \\ \boldsymbol{\omega} \end{pmatrix} = \begin{pmatrix} \boldsymbol{v} \\ \frac{1}{2}\boldsymbol{W}(\boldsymbol{\beta})^{T}\boldsymbol{\omega} \\ \frac{\boldsymbol{F}}{m_p} + g \\ \boldsymbol{I_p}^{-1}\boldsymbol{\tau} \end{pmatrix} \tag{1}$$

Here, $\boldsymbol{W}$ is the quaternion rate matrix as defined by Diebel [32], $\boldsymbol{F}$ is the vector sum of all aerodynamic forces acting on the puck (lift and drag), $\boldsymbol{I_p}$ is the puck's inertia tensor, and $\boldsymbol{\tau}$ is the vector sum of all aerodynamic moments acting on the puck (pitch and spin-down moments). m_p and g are constants representing the mass of the puck (0.170 kg) and the acceleration due to gravity (9.81 m/s^2). All forces, moments and tensors in equation (1) are expressed in the global co-ordinate system. The model predicts the complete trajectory of the puck by solving equation (1), with the initial values of $\boldsymbol{r}, \boldsymbol{\beta}, \boldsymbol{v}$ and $\boldsymbol{\omega}$ measured during initial flight phase.

Equations (2) – (3) describe lift and drag, two aerodynamic forces acting on the puck in flight:

$$F_d = -\frac{1}{2} C_D \rho A_p v^2 \hat{V} \tag{2}$$

$$F_L = \frac{1}{2} C_L \rho A_p v^2 \hat{N} \tag{3}$$

Here, A_p is the cross-sectional area of the puck (0.0046 m^2) and ρ is the density of air. Local air temperature (T = 0.23 ± 1.17 °C) and relative humidity (RH = 40.8 ± 4.1 %) were measured and used to calculate ρ for each day of testing (ρ = 1.29 ± 0.01) using the OmniCalculator © air density calculator (available at https://www.omnicalculator.com/physics/air-density). C_D and C_L are drag and lift coefficients adopted from Bohm et al.'s 2007 wind tunnel testing [24]. In general, lift and drag coefficients are dependent on Reynold's number and angle of attack α. Bohm et al. performed wind tunnel testing of hockey pucks and found that C_D and C_L are independent of Reynold's number for wind velocities between 13-30 m/s (the range of observed shot velocities in that study) [24]. It was therefore assumed that lift and drag coefficients used in the current study are independent of Reynold's number. Bohm et al. measured C_D and C_L values in this velocity range for angles of attack between 0º and 80º, and these values have been adopted for this study [24].

In a 2005 study of disc-wing (a.k.a. Frisbee™) aerodynamics, Potts determined that the Magnus side force can be neglected for advance ratios (rim velocity/wind velocity) below 0.35 [33]. In Bohm et al.'s study, advance ratios between 0.07 and 0.35 were observed, so they chose to neglect the Magnus side force [24]. It was therefore assumed that the Magnus force could be neglected in the current study.

Equations (4) – (5) describe the pitch and spin decay moments acting on the puck:

$$T_M = \frac{1}{2} C_M \rho A_p \left(\frac{4r_p}{\pi}\right) v^2 \, \hat{S} \tag{4}$$

$$T_N = -C_N \omega_{Z'} \, \widehat{Z}' \tag{5}$$

Here, C_M is the pitch torque coefficient and C_N is the spin decay coefficient, adopted from Bohm et al. [24]. Pitch torque coefficients were determined as a function of angle of attack by wind tunnel testing performed by Bohm et al., while spin decay coefficients were determined using high speed video analysis of pucks in flight [24]. r_p is the radius of the puck (0.0381 m), and the $\frac{4r_p}{\pi}$ term in equation (4) represents the average chord length of a circle. Fig. 5 shows a sample plot of a puck's modelled trajectory.

4.4.3 – Model Evaluation

The 3D motion capture system's measured puck position was determined at a minimum distance of 6 m for near-targeted shots, and a minimum distance of 10 m for far-targeted shots. Distances of 6 m and 10 m were selected because these were the maximum distances at which most shots had visible data. The first frame in which all three markers were visible, after the puck had travelled the minimum distance in the +Y direction from release, was defined as measured puck position ($\boldsymbol{M_x}$, $\boldsymbol{M_y}$, $\boldsymbol{M_z}$). The puck position at this Y co-ordinate was extracted from the model's predicted flight path, and defined as estimated puck position ($\boldsymbol{E_x}$, $\boldsymbol{E_y}$, $\boldsymbol{E_z}$). The difference between ($\boldsymbol{M_x}$, $\boldsymbol{M_y}$, $\boldsymbol{M_z}$) and ($\boldsymbol{E_x}$, $\boldsymbol{E_y}$, $\boldsymbol{E_z}$) was defined as model error ($\boldsymbol{D_x}$, $\boldsymbol{D_y}$, $\boldsymbol{D_z}$).

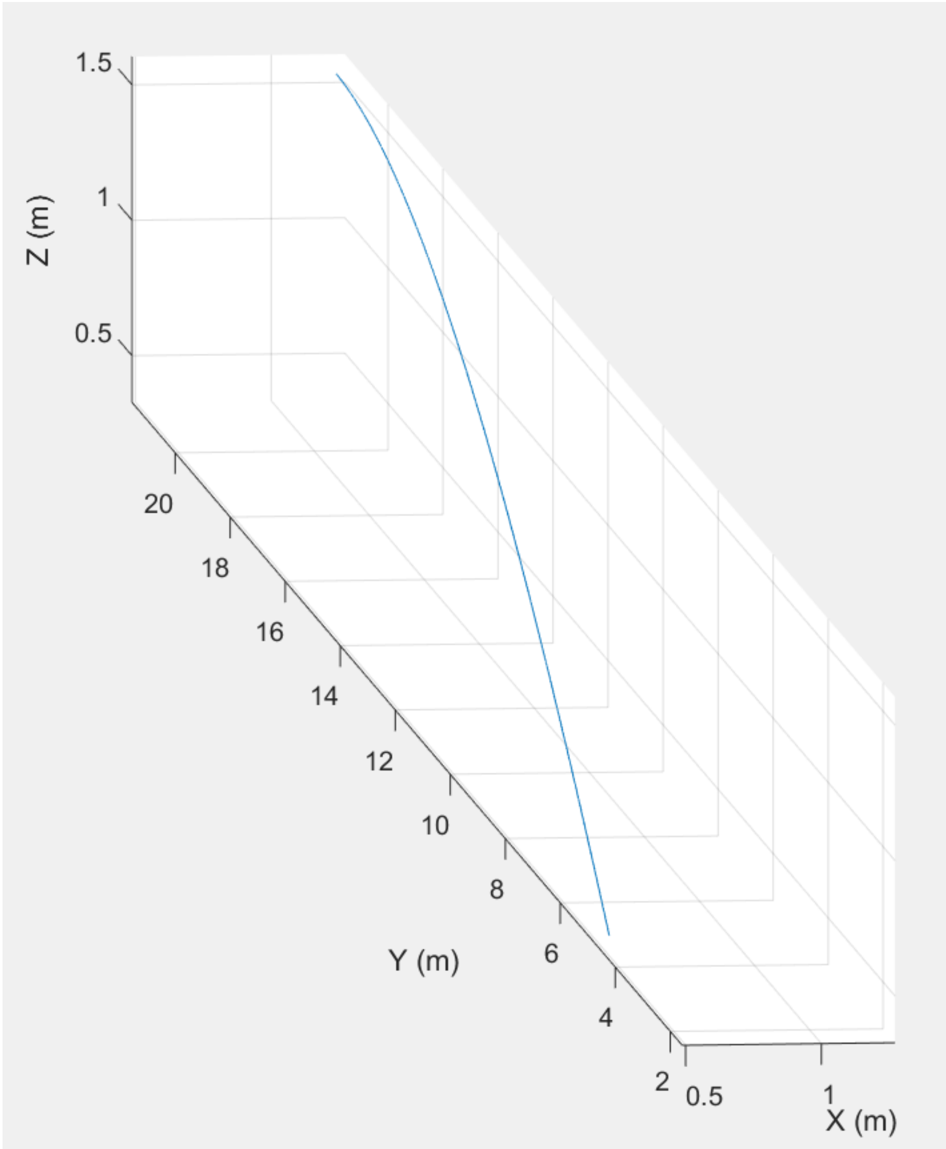

Fig. 5 Sample flight trajectory output from the simulation. The sample plot shows the trajectory of a near-target slap shot. X, Y and Z positions are shown in the global co-ordinate system.

4.4.4 – Exclusion Criteria

Shots were excluded from the analysis if one of the following conditions occurred:

- Insufficient Data – If any marker was not visible during the initial flight phase, or the puck's position could not be measured after travelling the minimum shot distance (as defined in section 4.4.3), shots were excluded.
- Measurement Error – To screen for obvious measurement errors, shots where $|\boldsymbol{v}|$ varied by more than 4.5 m/s during the initial flight phase were not included. 4.5 m/s corresponds to the average speed decrease for long shots, plus 3 standard deviations – this gives 99.7% certainty that these $\Delta|\boldsymbol{v}|$ values were measurement errors and not true values.
- Excessive Wobble – If $\widehat{Z}'$ varied by more than 30° during initial flight phase, shots were excluded. These shots cannot be accurately described by the aerodynamic model because of the rapid changes in force direction vectors. The cutoff of 30° corresponds to the mean change in $\widehat{Z}'$ plus two standard deviations.

Of the 360 shots recorded, 283 were included and 77 were excluded. 49 shots were excluded due to insufficient data, 5 were excluded due to measurement error and 23 were excluded due to excessive wobble.

4.5 - Statistical Analysis

The model's estimated puck position $\boldsymbol{E}$ and the measured puck position $\boldsymbol{M}$ were compared statistically using mean absolute error. MAE was chosen over RMSE as it is more easily interpreted [26] and the model's predictive parameters are not altered by error results, so RMSE is not necessary for least squares optimization [25]. The model's bias in the X and Z directions were evaluated using related samples t-tests comparing $\boldsymbol{E_x}$ to $\boldsymbol{M_x}$ and $\boldsymbol{E_z}$ to $\boldsymbol{M_z}$. Bland-Altman analysis was used to determine the model's limits of agreement with the 3D motion capture system [27]. Measured puck position $\boldsymbol{M}$ was used as the independent variable in the Bland-Altman analysis because position measurement by optical motion capture is considered a "gold standard" [34]. Additionally, the model's dependence on handedness of the shooter was assessed using independent samples t-tests comparing $\boldsymbol{D_x}$ and $\boldsymbol{D_z}$ for RHS and LHS.

4.6 – Sensitivity Analysis – Aerodynamic Forces

The puck's aerodynamic coefficients (C_L, C_D, C_M) were adopted from Bohm et al.'s wind tunnel testing, which occurred on pucks without reflective markers [24]. It was assumed that the placement of markers on the puck did not cause a significant aerodynamic effect [24]. Bohm et al. conducted wind tunnel testing of pucks both with and without reflective markers at a 0° angle of attack and it was found that the change in aerodynamic coefficients was less than 10% [24]. However, no analysis was conducted to determine the error in the model's predicted flight path as a result of these discrepancies.

In the present study, the model's sensitivity to changing aerodynamic coefficients was investigated by repeating the simulation for each shot with altered aerodynamic coefficients. The effect of lift, drag and pitch torque coefficients was analyzed individually by running the simulation with coefficients altered by ±10% of those determined by Bohm et al. [24]. Dependent samples t-tests were used to compare each altered model's final estimated puck position ($\boldsymbol{E_{x\text{-}alt}}$, $\boldsymbol{E_{z\text{-}alt}}$) with the unaltered model's estimated final puck position ($\boldsymbol{E_x}$, $\boldsymbol{E_z}$). An additional case with no aerodynamic forces was also performed, to gain an understanding of the magnitude of the aerodynamic forces' effect on the puck flight path.

5 - Results

5.1 – Measured Parameters

Each shot's velocity, spin rate and angle of attack were recorded in the initial flight phase. Table 2 shows these measured parameters for the 101 slap shots and 182 wrist shots included in the study. From release to target, puck velocity decreased by 1.74 ± 0.42 m/s for near shots and 2.96 ± 0.50 m/s for far shots.

Table 2 Measured shot parameters during the initial flight phase, reported as mean ± standard deviation

	Maximum Velocity (m/s)	**Spin Rate (rps)**	**Advance Ratio (rim velocity / wind velocity)**	**Angle of Attack (°)**
Slap Shots	31.4 ± 3.4	26.8 ± 4.6	0.21 ± 0.04	20.2 ± 6.0
Wrist Shots	29.0 ± 3.4	21.6 ± 4.1	0.18 ± 0.04	21.5 ± 7.7
All Shots	29.9 ± 3.6	23.6 ± 4.9	0.19 ± 0.04	21.0 ± 7.1

5.2 – Model Results

Initial flight phase data from each shot were input to the model and the trajectories were simulated. Table 3 shows the mean absolute error in the X and Z directions for each shot type and distance, as well as mean total error. Sample ($\boldsymbol{M_x}$, $\boldsymbol{M_z}$) and ($\boldsymbol{E_x}$, $\boldsymbol{E_z}$) data from a single participant's slap shots are displayed in Fig. 6. Fig. 7 shows the mean absolute error for near and far shots, in the X and Z directions.

Table 3 Mean absolute error between final measured puck position and the model's estimated final puck position

Shot Type	Shot Distance	Mean Absolute Error X (cm)	Mean Absolute Error Z (cm)	Mean Absolute Total Error (cm)
Wrist Shots	Near	2.31	2.44	3.80
	Far	6.07	5.23	8.86
Slap Shots	Near	3.35	2.26	4.58
	Far	5.24	4.39	7.63

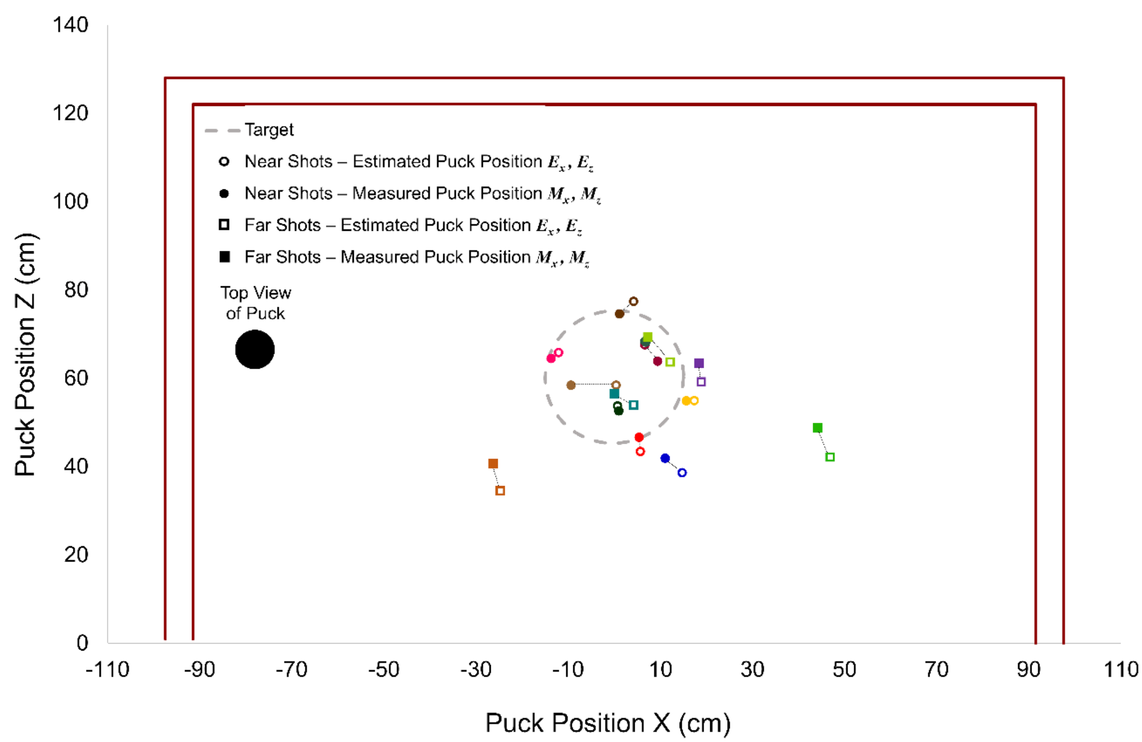

Fig. 6 Example of measured and estimated puck positions (M and E, respectively) for a single participant's slap shots. ***M*** and ***E*** for individual shot attempts are connected with a dotted line. The target and virtual net position is displayed for reference, based on the target being positioned directly in the center of the net

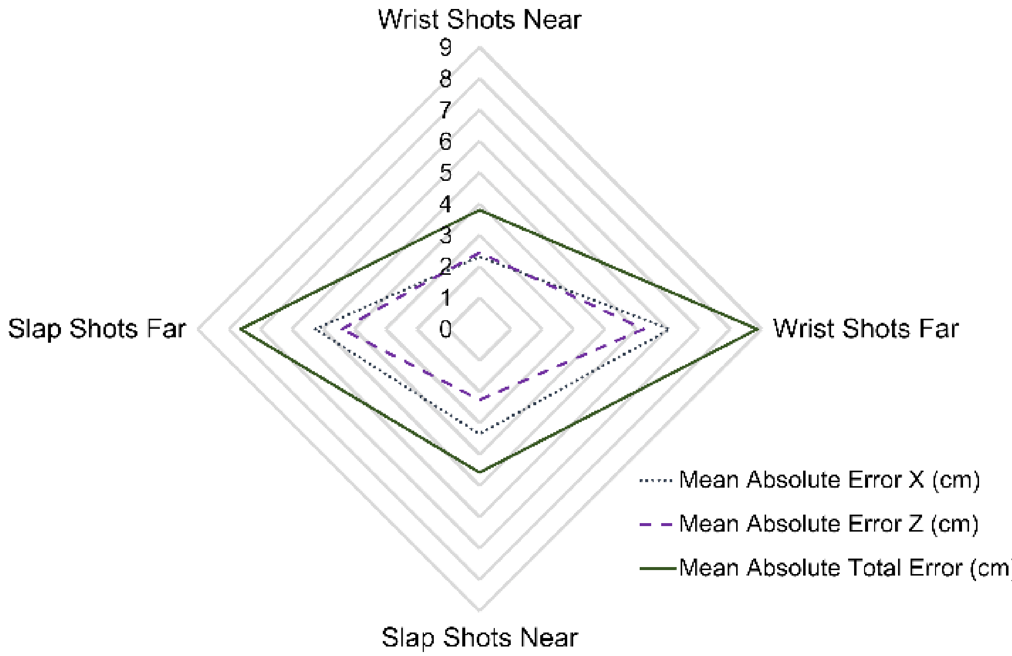

Fig. 7 Mean absolute error (cm) of the model's puck position estimates for each shot type (wrist and slap) and shot distance (near and far) combination

Related samples t-tests for all shots showed that measured position ($\overline{\boldsymbol{M}_x}$ = 0.016 ± 0.342 m) was not significantly different from estimated position ($\overline{\boldsymbol{E}_x}$= 0.019 ± 0.339 m) in the X direction; t(282)=-1.05, p=.297. However, a statistically significant difference between measured position ($\overline{\boldsymbol{M}_z}$ = 0.612 ± 0.233 m) and estimated position ($\overline{\boldsymbol{E}_z}$ = 0.603 ± 0.241 m) was found in the Z direction; t(282)=4.00, p<.001. This indicates that on average, the model underestimated the final height of the puck.

The model's bias and the 95% limits of agreement with the optical motion capture system are displayed on the Bland-Altman plots in Fig. 8 for near shots (a, c) and far shots (b, d). Table 4 lists the mean difference between measured and estimated shot location for each shot condition, along with the confidence intervals which indicate where 95% of the measurement differences are expected to lie.

Table 4: Bland-Altman analysis results. The mean difference between estimated final puck position and measured final puck position in the X and Z directions is shown for near and far shots, along with upper and lower 95% confidence intervals

	Mean (cm)	**Upper 95% CI (cm)**	**Lower 95% CI (cm)**
Near Shots – X direction	-0.03	7.48	-7.54
Far Shots – X direction	1.56	16.12	-13.00
Near Shots – Z direction	-1.00	4.82	-6.82
Far Shots – Z direction	-0.59	11.53	-12.71

Independent samples t-tests on model error did not reveal a statistically significant difference between model error for LHS ($\overline{\boldsymbol{D}_{z-LHS}}$ = -0.009 ± 0.039 m) and RHS ($\overline{\boldsymbol{D}_{z-RHS}}$ = -0.009 ± 0.038 m) in the Z direction; t(281)=-0.078, p=.938. However, a statistically significance between model error for LHS ($\overline{\boldsymbol{D}_{x-LHS}}$ = 0.015 ± 0.047 m) and RHS ($\overline{\boldsymbol{D}_{x-RHS}}$ = -0.018 ± 0.045 m) was found in the X direction; t(281)=5.669, p<.001.

No significant differences in model error were observed between wrist shots and slap shots. This includes near shots in the X direction; t(221)=-1.208, p=.228 and the Z direction; t(221) =-1.703, p=.090, as well as far shots in the X direction; t(57)=-1.203, p=.234 and the Z direction; t(57)=.913, p=.365.

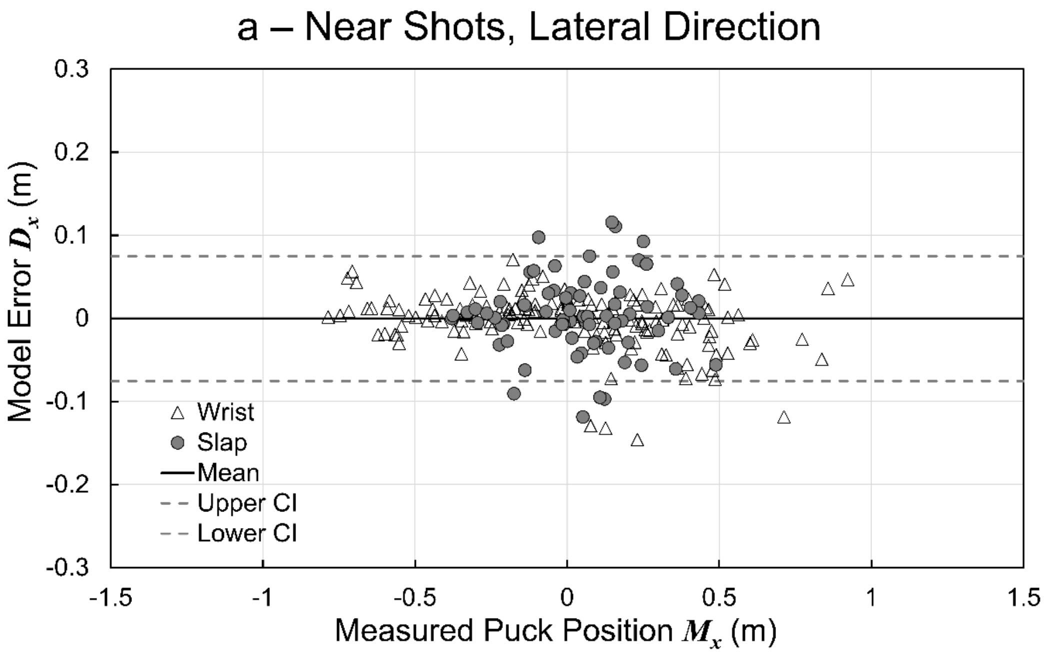
a – Near Shots, Lateral Direction
0.3
0.2
0.1
0
-0.1
-0.2
-0.3
Model Error D_x (m)
Wrist
Slap
Mean
Upper CI
Lower CI
-1.5
-1
-0.5
0
0.5
1
1.5
Measured Puck Position M_x (m)

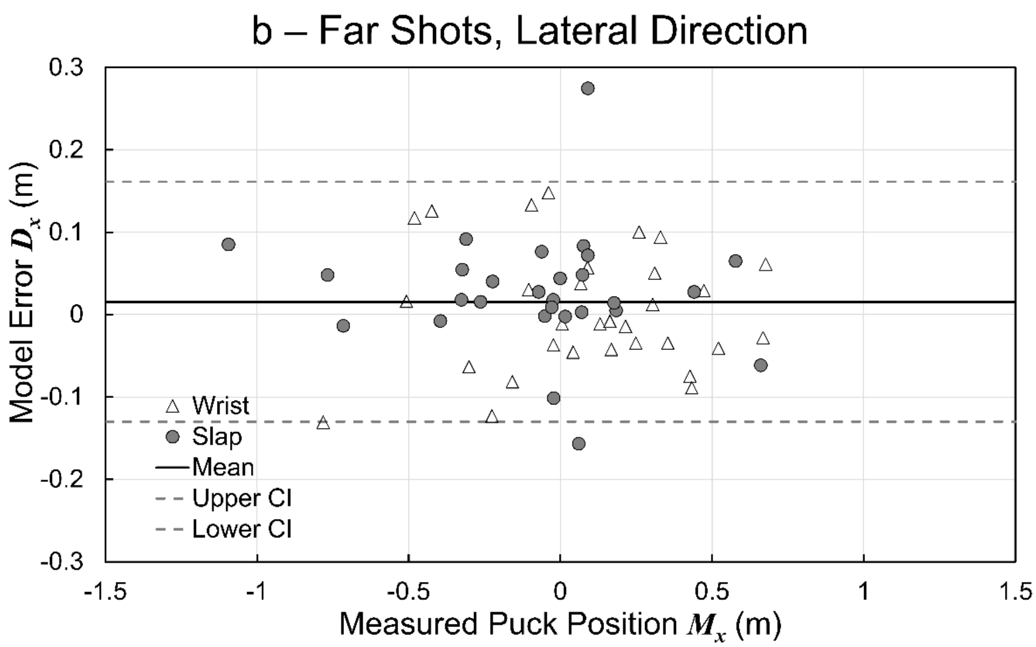
b – Far Shots, Lateral Direction
0.3
0.2
0.1
0
-0.1
-0.2
-0.3
Model Error D_x (m)
Wrist
Slap
Mean
Upper CI
Lower CI
-1.5
-1
-0.5
0
0.5
1
1.5
Measured Puck Position M_x (m)

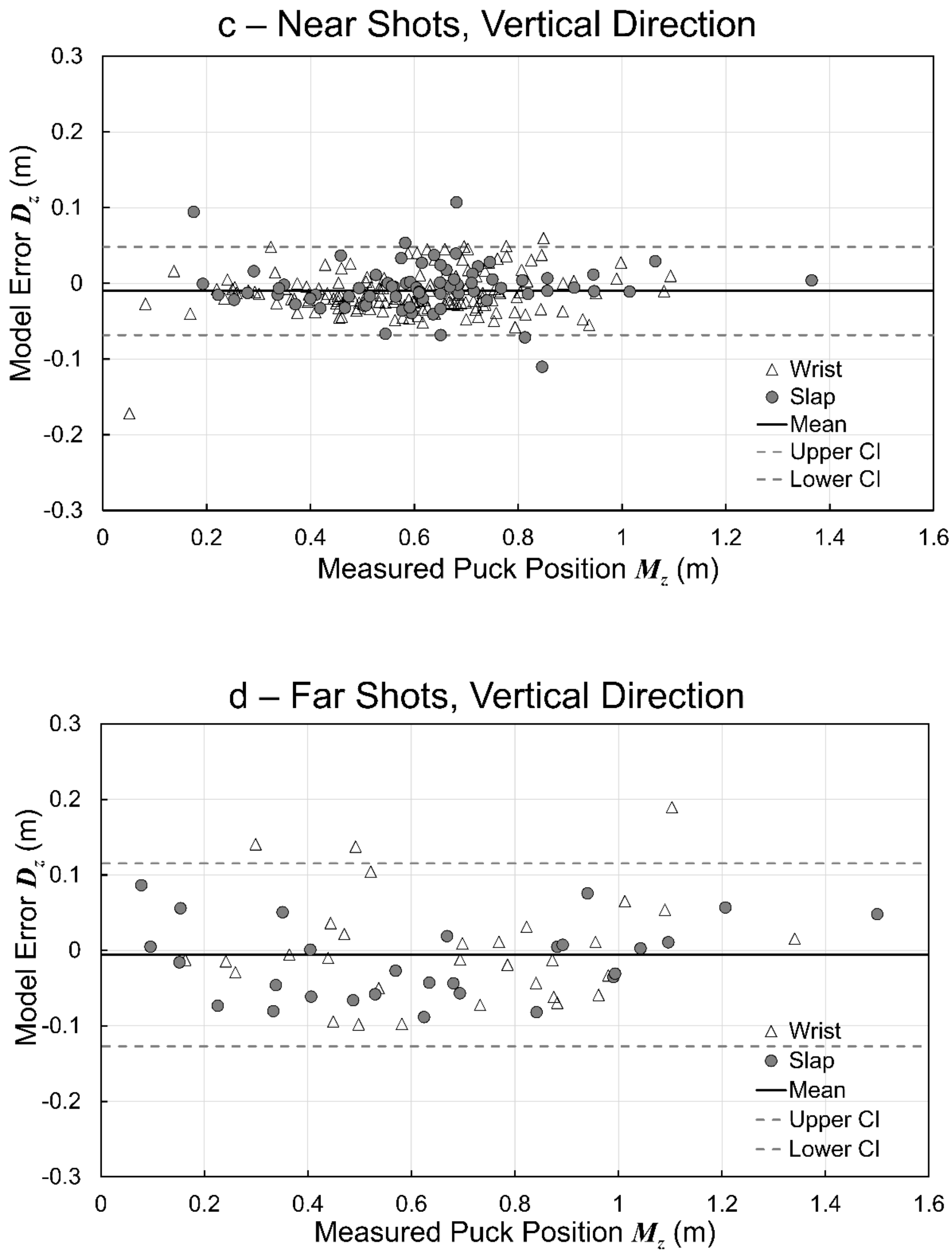

Fig. 8a-d Bland-Altman plots displaying model error plotted against measured puck position for both X (a,b) and Z (c,d) directions. a and c display near shots while b and d display far shots. Model bias is shown graphically as the mean model error $\bar{\boldsymbol{D}}$, and limits of agreement are shown as the upper and lower 95% confidence intervals, $CI = \bar{\boldsymbol{D}} \pm 1.96 * SD$

5.3 – Sensitivity Analysis - Aerodynamic Forces

The simulation was repeated for all shots with aerodynamic coefficients ±10% of the original values. Table 5 shows the results of independent samples t-tests on near-targeted shots comparing the original model's estimated final position in the Z direction (***E_z***) to each altered model's estimated final position in the Z direction (***$E_{z\text{-}alt}$***). Table 6 shows the corresponding results for far-targeted shots.

Table 5 Changes in the model's estimated final position due to altered aerodynamic coefficients for near shots in the Z direction

Condition	Mean Difference ± SD (cm)	t (221)	p value
No Forces	5.308 ± 1.994	39.656	<0.001
C_L + 10%	-0.586 ± 0.221	-39.484	<0.001
C_L - 10%	0.568 ± 0.214	39.559	<0.001
C_D + 10%	0.040 ± 0.022	27.996	<0.001
C_D - 10%	-0.059 ± 0.030	-28.956	<0.001
C_M + 10%	-0.043 ± 0.040	-16.065	<0.001
C_M - 10%	-0.063 ± 0.032	-29.246	<0.001

Table 6 Changes in the model's estimated final position due to altered aerodynamic coefficients for far shots in the Z direction

Condition	Mean Difference ± SD (cm)	t (58)	p value
No Forces	6.883 ± 10.765	4.912	<0.001
C_L + 10%	-1.790 ± 0.481	-28.574	<0.001
C_L - 10%	1.647 ± 0.420	30.155	<0.001
C_D + 10%	0.203 ± 0.085	18.417	<0.001
C_D - 10%	-0.347 ± 0.137	-19.473	<0.001
C_M + 10%	-0.350 ± 0.134	-20.153	<0.001
C_M - 10%	-0.344 ± 0.157	-16.782	<0.001

To investigate Bohm et al.'s assumption that the model results will not be substantially affected by 10% changes in aerodynamic coefficients, the combined case that resulted in the largest mean difference (C_L + 10%, C_D - 10%, C_M - 10%) was simulated. Table 7 shows the results of the dependent samples t-tests between the base model and this "Worst Case Scenario".

Table 7 "Worst Case Scenario" for altered aerodynamic coefficients. The mean difference of estimated final puck position in the Z direction between the base case and the (C_L + 10%, C_D - 10%, C_M - 10%) case is shown for near-targeted and far-targeted shots

Shot Distance	Mean Difference ± SD (cm)	t	p value
Near	-0.625 ± 0.238	$t(221) = -39.166$	<0.001
Far	-1.982 ± 0.530	$t(58) = -28.717$	<0.001

6 – Discussion

The model's mean absolute error is 3.8-4.6 cm over a distance of 6 meters and 7.6-8.9 cm over a distance of 10 meters. Hence, this model can offer a substantial improvement on current binary (hit/miss) shot accuracy metrics, and can be used to quantify shot accuracy in future ice hockey shooting studies and training tools. The physical model and aerodynamic parameters introduced by Bohm et al. [24] have been shown to be valid within an average absolute error of less than one puck diameter for shots on ice, over shot distances typically observed in ice hockey game play. However, the model could be refined by correcting potential sources of error and bias.

As indicated by the statistically significant bias in the -Z direction, on average the model under-predicts the final height of the puck by 0.9 cm. This suggests that lift force magnitudes applied in the model underestimate the actual lift forces. It was observed that altering aerodynamic coefficients by 10% can change model output by an average of up to 1.5 cm. Hence, refinement of the lift and pitch torque coefficients may correct the model's systematic bias. Bohm et al. performed wind tunnel testing of pucks with angle of attack from 0°-80° in increments of 10°, so considerable interpolation was required to determine the aerodynamic coefficients as a function of angle of attack. 95% of shots observed in this study had angles of attack between 6°-35°, so angular resolution of aerodynamic coefficients should be improved in this range. Further wind tunnel testing at smaller increments of angle of attack would be necessary to improve the resolution of aerodynamic coefficients. Additionally, wind tunnel testing on pucks with markers could improve the accuracy of the aerodynamic forces applied in the model.

When comparing overall model results including both LHS and RHS, the model did not show statistically significant bias in the X direction. However, statistically significant bias was observed in the X direction when shots were filtered by handedness of the shooter. On average, the model's predicted puck position for LHS was 1.46 cm right of the measured position, and 1.78 cm left of measured position for RHS. The model tends to predict that the pucks stays on a direct path in the X-Y plane from initial launch to final target, because the model fails to consider sideward aerodynamic force.

This result is evidence that the Magnus side force should not have been neglected. During the shot, the puck rolls from the heel of the stick blade towards the toe, causing the puck to rotate about the +Z axis for LHS, and the -Z axis for RHS. The Magnus force will therefore push the puck in the -X direction for LHS and the +X direction for RHS - this aligns with the direction of the model's bias in the lateral direction between LHS and RHS. The Magnus force was assumed to be negligible based on disc-wing wind tunnel tests [33], but this assumption was not verified for ice hockey pucks [24]. The Magnus force has been observed and studied in baseball [20], rugby [21] soccer [23] and for other sports projectiles [17] so it is reasonable to hypothesize that the Magnus force can also cause a measurable effect on ice hockey pucks in flight.

Proper quantification of the Magnus force would require wind tunnel testing with rotating ice hockey pucks to determine the Magnus force coefficient as a function of advance ratio and angle of attack. Until this is realized, future iterations of the model should include a correction factor that is proportional to advance ratio, to approximate the effects of the Magnus force.

The assumption of aerodynamic coefficients being independent of Reynold's number is a potential source of error. Bohm et al. observed shot velocities of up to 30 m/s and verified that aerodynamic coefficients were independent of Reynold's number at this velocity [24]. However, the current study included shots with velocities up to 37 m/s; this discrepancy was likely due to the current study's dynamic on-ice skating shots, which are shown to be faster than shots taken while stationary [35] [36]. Since wind tunnel testing was not performed at velocities up to 37 m/s, it was assumed that aerodynamic coefficients are still independent of Reynold's number at this velocity.

It was observed that a model which includes no aerodynamic forces would underestimate the final puck position in the Z direction by an average of 5.3 cm for near-targeted shots and 6.8 cm for far-targeted shots. This represents 0.9% and 0.7% of the total flight distance respectively, which is consistent with Bohm et al.'s finding that aerodynamic forces altered their puck flight simulation's final Z position by an average of 1.8 cm for a 3 meter shot (0.6% of total flight distance) [24]. The exclusion of aerodynamic forces effectively increases the error of the model by 225% for near shots and 140% for far shots.

Based on Bohm et al.'s finding that the aerodynamic coefficients do not change by more than 10% at a 0° angle of attack, two of the assumptions that are used in converting wind tunnel test results to aerodynamic coefficients are as follows:

1. The ±10% variation in aerodynamic coefficients will not have an appreciable effect on the model's results.
2. The markers will also cause the aerodynamic coefficients to vary by less than ±10% at all other angles of attack.

Comparing the base model to cases with ±10% altered aerodynamic coefficients resulted in a worst-case Z direction mean difference of 0.625 cm for near shots and 1.982 cm for far shots – this represents 26% and 41% of the base model's mean absolute error in the Z direction. Hence, the ±10% variation in aerodynamic coefficients has an appreciable effect on the model. Furthermore, the second assumption has not been tested or verified. Though it is expected that a 0º angle of attack would cause the markers to have the greatest aerodynamic effect (because their effective surface area is maximized at a 0º angle of attack), this assumption is not verified by empirical evidence. To enhance the accuracy of future iterations of the model, wind tunnel testing should be performed with reflective markers attached to the pucks.

For Bland-Altman analysis and quantification of the model's error, it was assumed that the error in the motion capture system's measurement of marker position was negligible. There is some error in optoelectronic measurement systems, arising from error in photogrammetric calibration, model reconstruction, electronic noise and the digitizing process of marker images [37]. However, Vicon systems have been shown to have mean errors of less than 1 mm [38–40], which is approximately two orders of magnitude less than the model's mean error. Furthermore, optical motion capture is considered the "gold standard" for motion capture technology [40] and therefore it is reasonable to neglect the error of these systems for analysis of a model with much larger mean error magnitudes.

A potential source of error in the motion capture system measurement is the high speed of the markers. At a given frame rate, the camera shutter will remain open for some amount of time. During this time, a marker will move – this means that the marker does not have a single position for any frame in which the marker is in motion. For a shot travelling at 30 m/s and using a camera operating at a shutter duration of 50 ms (the maximum shutter duration at a frame rate of 240 Hz), a marker could move up to 1.75 cm while the shutter is open. However, Vicon's algorithm uses a circle fitting algorithm that accounts for motion of the marker, and computes the centroid of this circle. In other words, the algorithm calculates the average position of the marker during the time in which the shutter is open. To the best knowledge of this author, the accuracy of motion capture systems at speeds up to 37 m/s has not been investigated. However, in a study of Vicon's positioning accuracy for robotics applications, it was seen that at low speeds (1-8 m/s) the mean error decreased with increasing linear velocity [38]. Further studies would be required to precisely quantify the error of the motion capture system at high speed.

The model is limited in its ability to predict the trajectory of shots with excessive wobble. The aerodynamic forces cannot be applied in the correct direction because the orientation vector is taken as a time-average over the initial flight phase. Pucks with high wobble have a periodically varying vector in the $\widehat{Z}'$ direction with a frequency much lower than the spin rate of the puck. Taking a time average of the $\widehat{Z}'$ direction vector over the 54 ms flight phase causes a sampling error because the puck may only undergo 1-2 "wobble cycles" in the initial flight phase. Therefore, the time average of the $\widehat{Z}'$ direction in the initial flight phase may not correctly represent the average orientation of the puck over the course of the flight. It is potentially possible to truncate the initial flight phase data to a single wobble cycle and use this truncated signal to find the average orientation vector. However, this may lead to increased error because the model assumes that the puck only rotates about the Z' axis, and wobbling pucks have non-negligible rotations about the X' and Y' axes. The effect of puck wobble on model accuracy could be further investigated.

However, the practicality of the model is not greatly affected by its inability to predict shots with excessive wobble, because these shots can easily be flagged and their results can be discarded. In a research setting, these shots can be considered "bad trials" and discarded, as was done in the current study. In a practice/coaching tool, the simulator can be programmed to display an error message to the user indicating that the shot could not be simulated due to excessive wobble. Fortunately, shots with excessive wobble are considered undesirable in ice hockey, so the model's practicality is not greatly affected by its inability to predict such shots.

Despite the limitations, the current model is valid within a mean absolute total error of less than 5 cm at 6 m and 9 cm at 10 m. Modelling puck trajectory can offer new accuracy-based metrics for precise quantification of shot outcomes, and these accuracy metrics can be useful for researchers as well as equipment manufacturers. Extensions of the current study would be to investigate the contributing factors to shooting accuracy: body kinematics, co-ordination patterns, kinetics (grip forces and grip force coupling), and equipment factors (shaft stiffness, blade patterns, etc.). Many of these factors have been studied in terms of their contribution to shot speed [2–4, 10, 30] but have not been assessed with respect to shot accuracy.

Additionally, the puck flight model to be incorporated into a real-time feedback tool for players and coaches, which could augment training engagement and specificity. Shot accuracy metrics like radial distance, RMS error and grouping size could be calculated and displayed in real time for shots taken on ice, or in off-ice training facilities. For a sample of a report that could be generated for a player seeking to analyze their shot accuracy, see Appendix B. Another potential application of the model is a shot simulator with visual presentation of virtual puck trajectory and net target zone (Fig. 9), which could be incorporated into a virtual reality experience for fans or used as a practice tool for players. Finally, future studies of dynamic on-ice shooting tasks can simultaneously measure body kinematics and shot accuracy with a limited field of view.

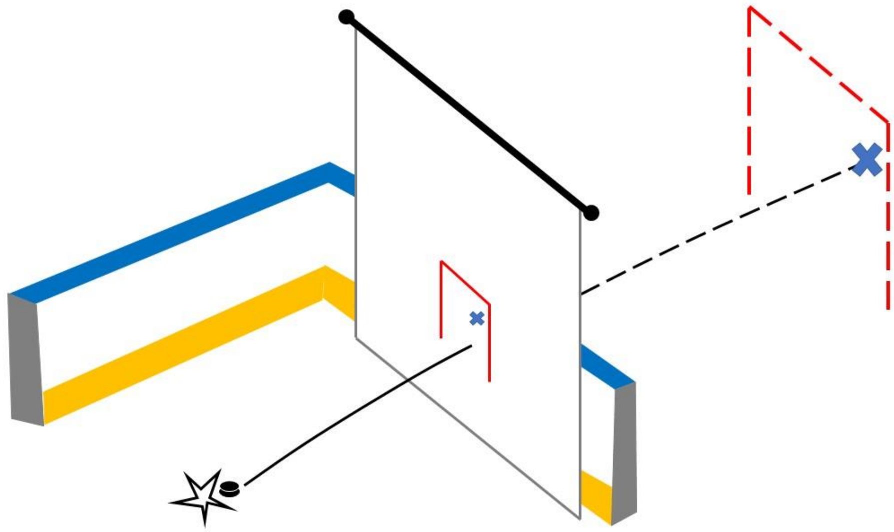

Fig. 9 Whiteboard display of final puck position (X) of a shot towards a virtual target net (--- ---)

7 – Conclusion

Ice hockey shot trajectory was modelled using Newton-Euler equations for a rigid body in flight. The model used conditions from the first 54 ms of flight to simulate the complete shot trajectory and compare the final position of the puck relative to a target. This model was shown to predict puck position within 5 cm mean absolute error (or less than a puck's diameter), for dynamic on-ice wrist shots and slap shots travelling up to 10 meters. The mean total errors of 3.80 cm for near wrist shots, 4.58 cm for near slap shots, 8.86 cm for far wrist shots and 7.63 cm for far slap shots are 0.8-3.86 cm greater than the objective of 0.5% of total flight path, but could be reduced by correcting for biases in the model.

The model had a statistically significant bias in the downward direction for all shots, indicating that the lift force is underestimated in the model. It was found that the model did not show significant differences between wrist shots and slap shots, but the model did have significant differences between RHS and LHS. The difference between LHS and RHS is evidence that the Magnus force caused measurable changes in the puck's trajectory and should be included in future models of ice hockey puck flight. The current model may be used as a tool in ice hockey shooting research and player development to measure shot accuracy with a high degree of precision.

Appendix A – Regression Approach to Bland-Altman Analysis

Proportional bias between model error $\boldsymbol{D}$ and measured position $\boldsymbol{M}$ is an indication of how the model's error depends on shot location. To investigate the model's proportional bias, regression analysis was performed on all shots in both the X and Z directions. Each plot was fit to the regression line given in equation (6):

$$\widehat{\boldsymbol{D}} = \overline{\boldsymbol{D}} + \mathrm{c}\boldsymbol{M} \tag{6}$$

Here, $\overline{\boldsymbol{D}}$ is the model's mean error and c is the slope of the regression line. If this regression is statistically significant, then the model's error has a dependence on the shot location [27].

Statistically significant regression was found in the X direction, with a proportional bias of c = -0.02 ± 0.01 (p=0.015). Statistically significant regression was also found in the Z direction, with proportional bias of c = 0.02 ± 0.01 (p=0.043).

While the model's proportional bias is statistically significant, the practical effect is relatively small. In the Z direction, the proportional bias of c = 0.02 ± 0.01 means that for every cm increase in measured height of a shot, the model error is expected to increase by 0.02 cm. Of all recorded shots, the average shot deviated from the target by 22 ± 16 cm in the Z direction – therefore, the model's error is expected to increase by an average of 0.44 cm due to proportional bias in the Z direction.

In the Z direction, the proportional bias causes the model to under-estimate the height of low shots and over-estimate the height of high shots. As seen in Section 5.3, changing aerodynamic coefficients can affect model results. Therefore, higher resolution of aerodynamic coefficients for angles of attack between 6°-35° could potentially eliminate the proportional bias in the Z direction.

Exclusion of the Magnus force could explain the model's proportional bias in the X direction. The proportional bias caused the model to under-predict deviations from the target – the model was more likely to err to the right for shots that missed the target to the left, and err to the left for shots that missed the target to the right. It was also observed that LHS were more likely to have shot deviations to the left of the target ($\overline{\boldsymbol{M}_{x-LHS}}$ = -10.3 ± 32.9 cm) while the opposite was true for RHS ($\overline{\boldsymbol{M}_{x-RHS}}$ = +23.0 ± 24.9 cm). As seen in Section 5, the model's average error is rightward for LHS and leftward for RHS. Therefore, the model's dependence on shot location in the X direction may have the same source as the model's dependence on handedness of the shooter. Hence, inclusion of the Magnus force could eliminate the proportional bias in the X direction.

Appendix B – Sample Shot Accuracy Report

Shooting Accuracy Report

Player: P01
Testing Date: Jan 18, 2019

	Wrist		Slap	
	Near	Far	Near	Far
Mean Left-Right Distance (cm)	25.1	48.7	5.3	-5.7
Mean Vertical Distance (cm)	26.0	27.9	-30.6	-69.0
Mean Radial Distance (cm)	44.6	60.8	37.4	74.7
Grouping Size (cm)	134.9	51.0	76.4	56.3
Mean Shot Velocity (m/s)	25.5	26.1	26.8	27.6

Target Height = 76 cm   Target Diameter = 33 cm
Mean Left-Right Distance: Average horizontal distance from the center of the target (negative numbers are left of the target, positive numbers are right of the target)
Mean Vertical Distance: Average vertical distance from the center of the target (negative numbers are below the target, positive numbers are above the target)
Mean Radial Distance: Average total distance from the center of the target
Grouping Size: Diameter of the smallest circle that contains all shots

Breakdown by Quadrant	
	% Shots
On Target	10%
Bottom Left	13%
Bottom Right	17%
Top Left	10%
Top Right	50%

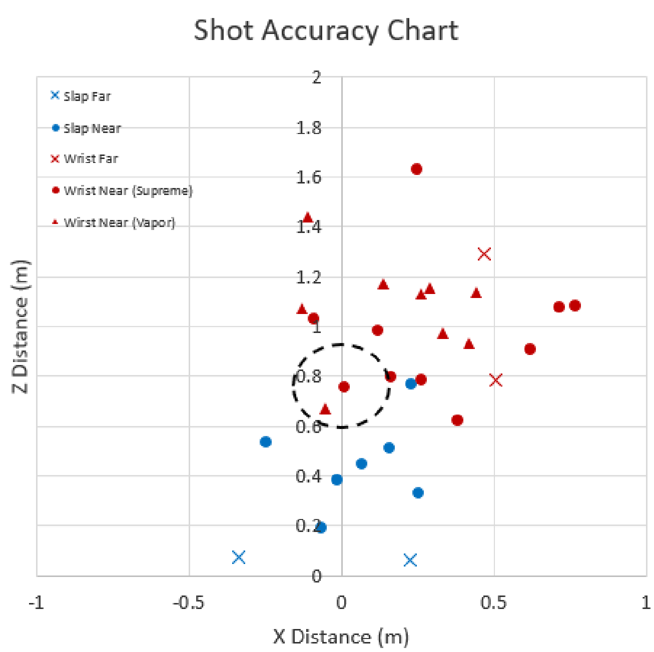

Average Values for All Study Participants

	Wrist		Slap	
	Near	**Far**	**Near**	**Far**
Mean Left-Right Distance (cm)	0.0	6.8	8.5	0.4
Mean Vertical Distance (cm)	-3.3	1.7	-8.0	0.9
Mean Radial Distance (cm)	45.1	60.3	31.3	60.2
Grouping Size (cm)	156.6	134.1	155.1	158.9
Mean Shot Velocity (m/s)	28.9	30.1	31.5	32.4

Appendix C – Technical Note on Data Collection Setup

In the current study, the target was inside the camera's capture volume and reflective markers were placed on the target. This made it simple to determine the position of the puck relative to the target. However, future studies that incorporate this model may not have the target in the field of view. It will therefore be necessary to include a reference marker in the field of view, at a location that is fixed for all trials. The displacement vector from the center of the target to the reference point in the global X-Y-Z co-ordinate system must be measured, and incorporated into the "shotzero.m" MATLAB script. A sample script is shown at the end of this Appendix, where the reference marker is measured to be 2 meters from the target's center in the -X direction, 0.76 meters from the target in the -Z direction, and an input variable "d_target" meters from the target in the -Y direction.

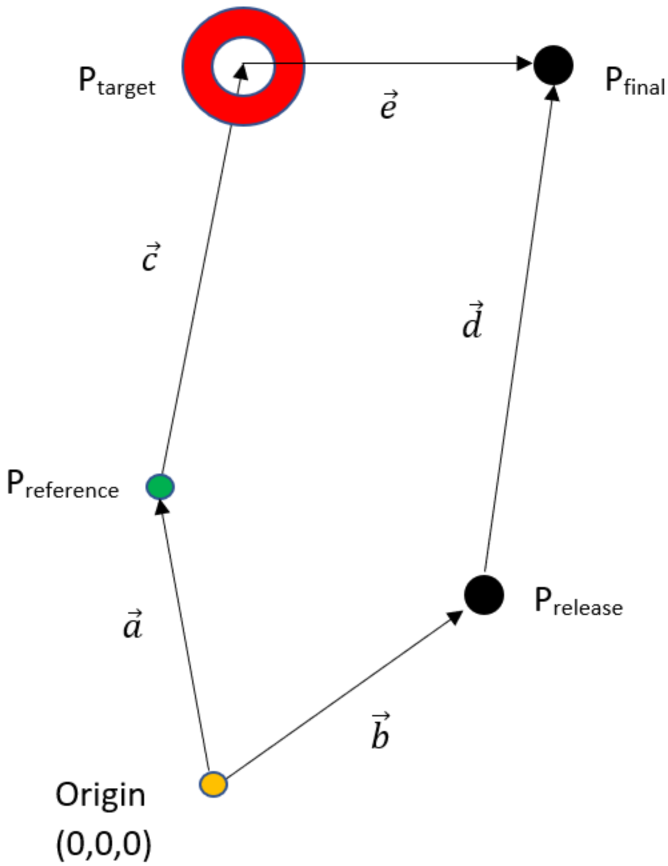

Fig. 10 Depiction of the measured and calculated vectors required to determine the relative position of a puck to a target using a simulated puck flight.

Fig. 10 shows the measured and calculated position vectors used to calculate the final position of a shot relative to a target. Position vectors **a** and **b** are measured by the motion capture system. Vector **c** must be measured by the researcher prior to calibration – it is essential to measure the distances in alignment with the global X, Y and Z directions. Vector **d** is calculated by the puck flight simulation. The positions of the target is calculated as **a** + **c**, and the final puck position is calculated as **b** + **d**. The final position of the puck relative to the target can therefore be found using **e** = (**a** + **c**) – (**b** + **d**).

```
function[shot_zero,target,origin] = shotzero(shot,d_target)
% defines the target position relative to a reference point and removes
all frames before the puck is visible

%Position of reference marker
ref_x=mean(nonzeros(shot(:,24)));
ref_y=mean(nonzeros(shot(:,25)));
ref_z=mean(nonzeros(shot(:,26)));

idx_nonzero = find(shot(:,3)~=0 & shot(:,6)~=0 & shot(:,9)~=0, 1,
'first'); %find frame when all three markers are visible

shot(1:idx_nonzero,:) = []; % remove all frames before puck appears

frame = shot(:,1); %Defines puck position array variables
shot_zero(:,3)=shot(:,3);
shot_zero(:,4)=shot(:,4);
shot_zero(:,5)=shot(:,5);
shot_zero(:,6)=shot(:,6);
shot_zero(:,7)=shot(:,7);
shot_zero(:,8)=shot(:,8);
shot_zero(:,9)=shot(:,9);
shot_zero(:,10)=shot(:,10);
shot_zero(:,11)=shot(:,11);

%Define the position of the target relative to the reference point
target(1) = ref_x + 2000;
target(2) = ref_y + d_target*1000; %y distance from origin to target
target(3) = ref_z + 760; %height of target

target = target/1000; %convert to m

end
```

Appendix D – Additional Figures

Fig. 11a-b shows the model error in the X direction for near and far shots, grouped by handedness of the shooter. These plots offer a visualization of the data which clearly shows the tendency of the model to have errors in the +X direction for LHS and the –X direction for RHS. This is likely due to the Magnus force, which was not accounted for in the current model.

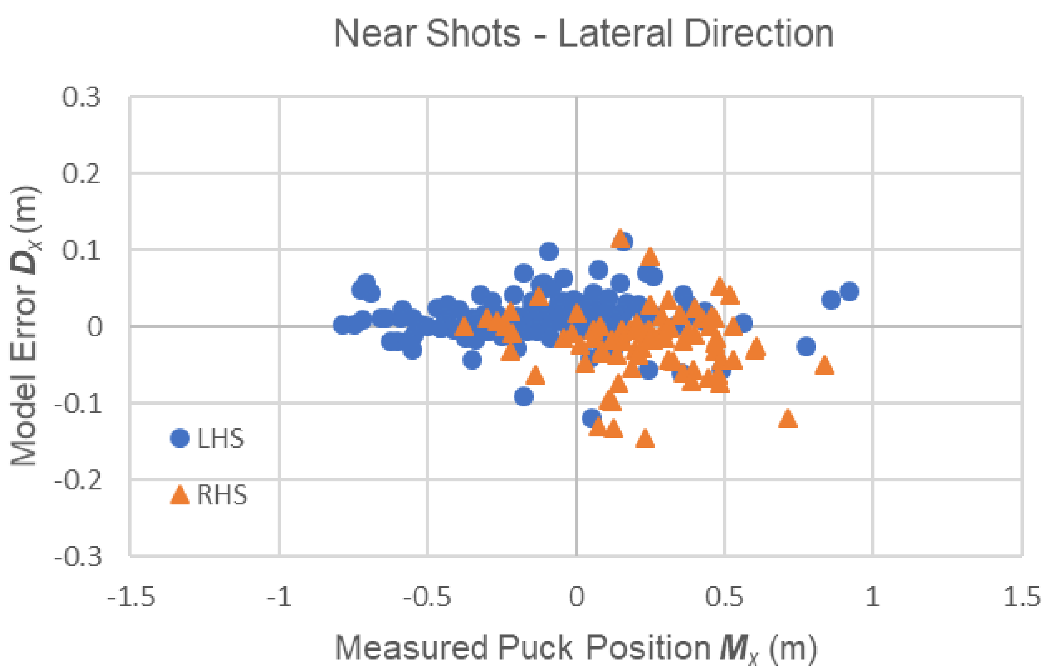

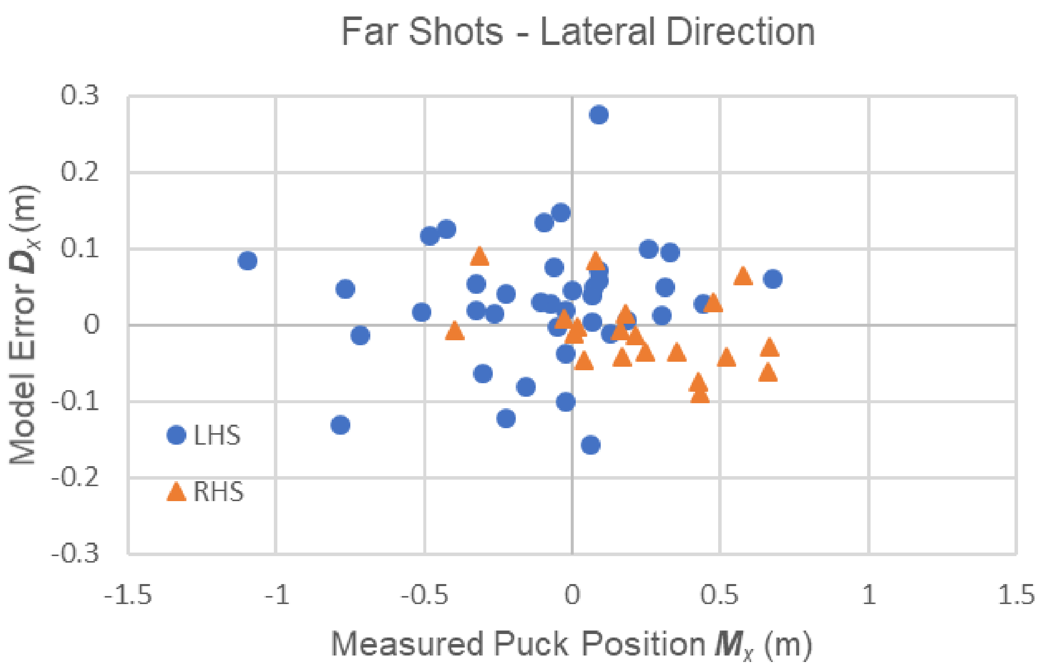

Fig. 11a-b Model error for near (a) and far (b) shots in the lateral direction, plotted against measured puck position in the lateral direction. Data is grouped by LHS and RHS.

References

1. Worobets JT, Fairbairn JC, Stefanyshyn DJ (2006) The influence of shaft stiffness on potential energy and puck speed during wrist and slap shots in ice hockey. Sport Eng 9:191–200
2. Villaseñor A, Turcotte RA, Pearsall DJ (2006) Recoil effect of the ice hockey stick during a slap shot. J Appl Biomech 22:200–209. https://doi.org/10.1123/jab.22.3.202
3. Wu T-C, Pearsall D, Hodges A, et al (2003) The performance of the ice hockey slap and wrist shots: the effects of stick construction and player skill. Sport Eng 6:31–39. https://doi.org/10.1007/BF02844158
4. Pearsall DJ, Montgomery DL, Rothsching N, Turcotte RA (1999) The influence of stick stiffness on the performance of ice hockey slap shots. Sport Eng 3–12
5. Michaud-Paquette Y, Pearsall DJ, Turcotte RA (2009) Predictors of scoring accuracy: ice hockey wrist shot mechanics. Sport Eng 11:75–84. https://doi.org/10.1007/s12283-008-0009-9
6. Michaud-Paquette Y, Pearsall DJ, Turcotte R (2011) Whole-body predictors of wrist shot accuracy in ice hockey : A kinematic analysis. Sport Biomech 10:10–21. https://doi.org/10.1080/14763141.2011.557085
7. Carkeet A, Chan P, Brown B (1988) Vision in competition pistol shooters: effects of distance defocus on performance. Clin Exp Optom 71:60–65. https://doi.org/10.1111/j.1444-0938.1988.tb03750.x
8. Goonetilleke RS, Hoffmann ER, Lau WC (2009) Pistol shooting accuracy as dependent on experience , eyes being opened and available viewing time. Appl Ergon 40:500–508. https://doi.org/10.1016/j.apergo.2008.09.005

9. Scholz JP, Schoner G, Latash ML (2000) Identifying the control structure of multijoint coordination during pistol shooting. Exp Brain Res 135:382–404. https://doi.org/10.1007/s002210000540

10. MacInnis N (2019) Does X-Factor Exist in Ice Hockey Slap Shots ? Comparison of Elite versus Recreational Players Thorax to Pelvis Coordination

11. Renger R (1994) Identifying the Task Requirements Essential to the Success of a Professional Ice Hockey Player : A Scout ' s Perspective. J Teach Phys Educ 13:180–195

12. Marshall M (2015) Defenseman goal scoring analysis from the 2013-2014 National Hockey League season

13. Couture RT, Singh M, Lee W, et al (1996) Can mental training help to improve shooting accuracy ? Polic An Int J 22:696–711

14. Fitts PM (1954) The information capacity of the human motor system in controlling the amplitude of movement. J Exp Psychol 47:381–391

15. Looser J, Cockburn A, Savage J (2005) On the Validity of Using First-Person Shooters for Fitts' Law Studies. People Comput XIX:33–36

16. Brown AA, Coelho CJ (2017) Modeling goal-directed movements in modern pistol competition. In: IEEE International Conference on Systems, Man, and Cybernetics (SMC). pp 770–775

17. Goff JE (2014) A review of recent research into aerodynamics of sport projectiles A review of recent research into aerodynamics of sport projectiles. Sport Eng 16:137–154. https://doi.org/10.1007/s12283-013-0117-z

18. Hanna RK (2012) CFD in sport - A retrospective; 1992 - 2012. Procedia Eng

34:622–627. https://doi.org/10.1016/j.proeng.2012.04.106

19. Passmore MA, Tuplin S, Spencer A, Jones R (2008) Experimental studies of the aerodynamics of spinning and stationary footballs. Proc Inst Mech Eng Part C J Mech Eng Sci 222:195–205. https://doi.org/10.1243/09544062JMES655

20. Briggs LJ (1959) Effect of Spin and Speed on the Lateral Deflection (Curve) of a Baseball; and the Magnus Effect for Smooth Spheres. Am J Phys 27:589–596. https://doi.org/10.1119/1.1934921

21. Seo K, Kobayashi O, Murakami M (2006) Flight dynamics of the screw kick in rugby. Sport Eng 9:49–58. https://doi.org/10.1007/bf02844262

22. Nathan AM (2008) The effect of spin on the flight of a baseball. Am J Phys 76:119–124. https://doi.org/10.1119/1.2805242

23. Goff JE, Carré MJ (2009) Trajectory analysis of a soccer ball. Am J Phys 77:1020–1027. https://doi.org/10.1119/1.3197187

24. Böhm H, Schwiewagner C, Senner V (2007) Simulation of puck flight to determine spectator safety for various ice hockey board heights. Sport Eng 10:75–86

25. Chai T, Draxler RR, Prediction C (2014) Root mean square error (RMSE) or mean absolute error (MAE)? – Arguments against avoiding RMSE in the literature. 1247–1250. https://doi.org/10.5194/gmd-7-1247-2014

26. Willmott CJ, Matsuura K (2005) Advantages of the mean absolute error (MAE) over the root mean square error (RMSE) in assessing average model performance. Clim Res 30:79–82

27. Bland JM, Altman DG (1999) Measuring agreement in method comparison

studies. Stat Methods Med Res 8:135–160

28. Giavarina D (2015) Understanding Bland Altman analysis. Biochem Medica 25:141–151. https://doi.org/10.11613/BM.2015.015

29. Renaud PJ, Robbins SMK, Dixon PC, et al (2017) Ice hockey skate starts: a comparison of high and low calibre skaters. Sport Eng 20:255–256. https://doi.org/10.1007/s12283-017-0227-0

30. Pearsall DJ, Robbins SMK, Renaud PJ, et al (2018) On-Ice 3D Study of Wrist Shots. In: The Hockey Conference. p 3

31. Shell JR (2016) Skating propulsion: three-dimensional kinematic analysis of high caliber male and female ice hockey players

32. Diebel J (2006) Representing Attitude : Euler Angles , Unit Quaternions , and Rotation Vectors. Matrix 58:

33. Potts J (2005) Disc-wing Aerodynamics

34. Krouwer FJS (2008) Why Bland – Altman plots should use X , not (Y + X)/ 2 when X is a reference method. Stat Med 778–780. https://doi.org/10.1002/sim.3086

35. Doré R, Roy B (1976) Dynamometric analysis of different hockey shots. In: Proceedings of the Fourth International Congress on Biomechanics. pp 277–285

36. Alexander JF, Haddow JB, Schultz GA (1963) Comparison of the ice hockey wrist and slap shots for speed and accuracy. Res Quarterly Am Assoc Heal Phys Educ Recreat 34:259–266

37. Chiari L, Della Croce U, Leardini A, Cappozzo A (2005) Human movement analysis using stereophotogrammetry. Part 2: Instrumental errors. Gait Posture

21:197–211. https://doi.org/10.1016/j.gaitpost.2004.04.004

38. Merriaux P, Dupuis Y, Boutteau R, et al (2017) A study of vicon system positioning performance. Sensors (Switzerland) 17:1–18. https://doi.org/10.3390/s17071591

39. Spörri J, Schiefermüller C, Müller E (2016) Collecting kinematic data on a ski track with optoelectronic stereophotogrammetry: A methodological study assessing the feasibility of bringing the biomechanics lab to the field. PLoS One 11:. https://doi.org/10.1371/journal.pone.0161757

40. van der Kruk E, Reijne MM (2018) Accuracy of human motion capture systems for sport applications; state-of-the-art review. Eur J Sport Sci 18:806–819. https://doi.org/10.1080/17461391.2018.1463397